Ceramics-Silikáty 63 (3), 330-337 (2019)
www.ceramics-silikaty.cz doi: 10.13168/cs.2019.0028

TEMPERATURE-DEPENDENT PROPORTIONAL LIMIT STRESS OF CARBON FIBER-REINFORCED SILICON CARBIDE CERAMIC-MATRIX COMPOSITES

LI LONGBIAO

College of Civil Aviation, Nanjing University of Aeronautics and Astronautics
No.29 Yudao St., Nanjing 210016, PR China

#E-mail: llb451@nuaa.edu.cn

Submitted February 11, 2019; accepted April 25, 2019

Keywords: Ceramic-matrix composites (CMCs), Proportional limit stress, Interface debonding

In this paper, the temperature-dependent proportional limit stress of carbon fiber-reinforced silicon carbide ceramic-matrix composites (C/SiC CMCs) is investigated using the energy balance approach. The temperature-dependent micromechanical parameters of fiber and matrix modulus, fiber/matrix interface shear stress and interface debonded energy, and matrix fracture energy are incorporated into the analysis of the micro stress analysis, fiber/matrix interface debonding criterion and energy balance approach. The relationships between the proportional limit stress, fiber/matrix interface debonding and temperature are established. The effects of fiber volume fraction, fiber/matrix interface shear stress, interface frictional coefficient, interface debonded energy and matrix fracture energy on the proportional limit stress and fiber/matrix interface debonding length versus temperature curves are discussed. The experimental proportional limit stress and fiber/matrix interface debonding length of 2D C/SiC composite at elevated temperatures of 973 K and 1273 K are predicted. For C/SiC composite, the proportional limit stress of C/SiC composite increases with temperature, due to the increasing of fiber/matrix interface shear stress and decreasing of the thermal residual stress.

INTRODUCTION

With the development of aerospace industry, the requirements for high temperature, high specific strength and high specific modulus materials are getting higher. Ultra-high temperature, long-life lightweight thermal structural materials are the key prerequisites for the future development of aerospace engines to high performance, light weight, low emissions, and low noise. Ceramic matrix composites (CMCs) possess the advantages of high specific strength, high specific modulus, low density, good wear resistance and chemical resistance at elevated temperatures, making them the material of choice for replacing high temperature alloys in high thrust-to-weight ratio aero engines [1, 2, 3, 4, 5]. The mechanical properties of CMCs are much different from those of single-phase ceramics. In single-phase ceramics, the failure of materials is caused by the initiation and propagation of main cracks. The elastic modulus of the whole material does not change during this process. However, when the CMC is subjected to stress, there are many microscopic failure mechanisms generated inside of composite, i.e., matrix cracking, fiber/matrix interface debonding and fibers fracture, leading to the quasi-ductile behavior in tensile stress-strain curves [6, 7 and 8]. Specially, in CMCs the onset of nonlinearity, i.e., the proportional limit, does not represent the yield point and onset of work hardening as it does in metals [9]. Instead, in CMCs the proportional limit is often associated with the macroscopic manifestation of first matrix cracking. The proportional limit stress (PLS) is a more important property than fracture strength while the structural component is designed [10]. The factor of safety design is obtained by comparing the PLS with the applied stress state (σ) and the value of a safety design should be greater than one, i.e., $PLS/\sigma_a > 1$.

Many researchers performed experimental and theoretical investigations on matrix cracking in fiber-reinforced CMCs. The energy balance approach can be used to determine the steady-state matrix cracking stress, including the ACK model [11], AK model [12], BHE model [13], Kuo-Chou model [14], Sutcu-Hilling model [15], Chiang model [16], and Li model [17]; and the stress intensity factor method is adopted to determine the short matrix cracking stress, including the MCE model [18], MC model [19], McCartney model [20], Chiang-Wang-Chou model [21], Danchaivijit-Shetty model [22] and Thouless-Evans model [23]. Kim and Pagano [24], Dutton et al. [25] investigated the first matrix cracking in CMCs using the acoustic emission (AE), optical microscope and scanning electronic microscope (SEM). It was found that the experimental first matrix cracking stress is much lower than the theoretical results predicted by ACK model [11]. The micro matrix cracking appears

first in the matrix rich region, and with increasing applied stress, these micro matrix cracks propagate and stops at the fiber/matrix interface. In fact, these micro matrix cracks do not affect the macro strain and stiffness of CMCs [26], however, at higher applied stress, these micro matrix cracks evolve first into the short matrix cracking defined by MCE model [18], and then the steady-state matrix cracking defined by ACK model [11]. The steady-state matrix cracking model can be used to predict the PLS. However, in the studies mentioned above, the temperature-dependent proportional limit stress of fiber-reinforced CMCs has not been investigated.

In this paper, the temperature-dependent proportional limit stress of C/SiC composite is investigated using the energy balance approach. The temperature-dependent micromechanical parameters of fiber and matrix modulus, fiber/matrix interface shear stress and interface debonded energy, and matrix fracture energy are incorporated into the analysis of the micro stress analysis, fiber/matrix interface debonding criterion and energy balance approach. The relationships between the proportional limit stress, fiber/matrix interface debonding and temperature are established. The effects of fiber volume fraction, fiber/matrix interface shear stress, interface frictional coefficient, interface debonded energy and matrix fracture energy on the proportional limit stress and fiber/matrix interface debonding length versus temperature curves are discussed. The experimental proportional limit stress and fiber/matrix interface debonding length of 2D C/SiC composite at elevated temperatures of 973 K and 1273 K are predicted.

THEORETICAL

The energy balance relationship to evaluate the proportional limit stress of CMCs can be described using the following equation. [13]

$$\frac{1}{2}\int_{-\infty}^{\infty}\left\{\frac{V_f}{E_f(T)}\left[\sigma_{fu}(T)-\sigma_{fd}(T)\right]^2+\frac{V_m}{E_m(T)}\left[\sigma_{mu}(T)-\sigma_{md}(T)\right]^2\right\}dx+ +\frac{1}{2\pi R^2 G_m(T)}\int_{-l_d(T)}^{l_d(T)}\int_{r_f}^{R}\left[\frac{r_f\tau_i(x,T)}{r}\right]2\pi r dr dx= =V_m\gamma_m(T)+\frac{4V_f l_d(T)}{r_f}\gamma_d(T) \quad (1)$$

where V_f and V_m denote the fiebr and matrix volume fraction, respectively; $E_f(T)$ and $E_m(T)$ denote the temperature-dependent fiber and matrix elastic modulus, respectively; $\sigma_{fu}(T)$ and $\sigma_{mu}(T)$ denote the fiber and matrix axial stress distribution in the matrix cracking upstream region, respectively; $\sigma_{fd}(T)$ and $\sigma_{md}(T)$ denote the fiber and matrix axial stress distribution in the matrix cracking downstream region, respectively. $\gamma_m(T)$ and $\gamma_d(T)$ denote the temperature-dependent matrix fracture energy and interface debonded energy, respectively.

$$\sigma_{fu}(T)=\frac{E_f(T)}{E_c(T)}\sigma \quad (2)$$

$$\sigma_{mu}(T)=\frac{E_m(T)}{E_c(T)}\sigma \quad (3)$$

$$\sigma_{fd}(x,T)=\begin{cases}\dfrac{\sigma}{V_f}-\dfrac{2\tau_i(T)}{r_f}x, x\in\left[0,l_d(T)\right]\\ \dfrac{E_f(T)}{E_c(T)}\sigma, x\in\left[l_d(T),\dfrac{l_c(T)}{2}\right]\end{cases} \quad (4)$$

$$\sigma_{md}(x,T)=\begin{cases}2\dfrac{V_f}{V_m}\dfrac{\tau_i(T)}{r_f}x, x\in\left[0,l_d(T)\right]\\ \dfrac{E_m(T)}{E_c(T)}\sigma, x\in\left[l_d(T),\dfrac{l_c(T)}{2}\right]\end{cases} \quad (5)$$

$$l_d(T)=\frac{r_f V_m E_m(T)\sigma}{2V_f E_c(T)\tau_i(T)}-\sqrt{\frac{r_f V_m E_f(T)\gamma_d(T)}{E_c(T)\tau_i^2(T)}} \quad (6)$$

where [27]

$$\tau_i(T)=\tau_0+\mu\frac{|\alpha_{rf}(T)-\alpha_{rm}(T)|(T_m-T)}{A} \quad (7)$$

Substituting the upstream and downstream temperature-dependent fiber and matrix axial stresses of Equation 2, 3, 4 and 5, and the temperature-dependent fiber/matrix interface debonded length of Equation 6 into Equation 1, the energy balance equation leads to the following equation.

$$\alpha\sigma^2+\beta\sigma+\delta=0 \quad (8)$$

where

$$\alpha=\frac{V_m E_m(T)\,l_d(T)}{V_f E_f(T)\,E_c(T)} \quad (9)$$

$$\beta=\frac{2\tau_i(T)\,l_d(T)}{r_f E_f(T)}\,l_d^2(T) \quad (10)$$

$$\delta=\frac{4}{3}\left[\frac{\tau_i(T)}{r_f}\right]^2\frac{V_f E_c(T)}{V_m E_f(T)E_m(T)}l_d^3(T)-\frac{4V_f\gamma_d(T)}{r_f}-V_m\gamma_m(T) \quad (11)$$

RESULTS AND DISCUSSION

The ceramic composite system of C/SiC is used for the case study and its material properties are given by: $V_f = 30$ %, $r_f = 3.5$ μm, $\gamma_m = 25$ J·m^{-2} (at room temprature), $\gamma_d = 0.1$ J·m^{-2} (at room temperature).

The temperature-dependent carbon fiber elastic modulus of $E_f(T)$ can be described using the following equation. [28]

$$E_f(T)=230\left[1-2.86\times10^{-4}\exp\left(\frac{T}{324}\right)\right], T<2273\ \text{K} \quad (12)$$

The temperature-dependent SiC matrix elastic modulus of $E_m(T)$ can be described using the following equation. [29]

$$E_m(T) = \frac{350}{460}\left[460 - 0.04T\exp\left(-\frac{962}{T}\right)\right], T \in [300\text{K}\ 1773\text{K}] \quad (13)$$

The temperature-dependent carbon fiber axial and radial thermal expansion coefficient of $\alpha_{lf}(T)$ and $\alpha_{rf}(T)$ can be described using the following equations. [30]

$$\alpha_{lf}(T) = 2.529 \times 10^{-2} - 1.569 \times 10^{-4}\,T + 2.228 \times 10^{-7}\,T^2 - 1.877 \times 10^{-14}\,T^4, \quad T \in [300\text{K}\ 2500\text{K}] \quad (14)$$

$$\alpha_{rf}(T) = -1.86 \times 10^{-1} + 5.85 \times 10^{-4}\,T - 1.36 \times 10^{-8}\,T^2 + 1.06 \times 10^{-22}\,T^3, \quad T \in [300\text{K}\ 2500\text{K}] \quad (15)$$

The temperature-dependent SiC matrix axial and radial thermal expansion coefficient of $\alpha_{lm}(T)$ and $\alpha_{rm}(T)$ can be described using the following equations. [29]

$$\alpha_{lm}(T) = \alpha_{rm}(T) = \begin{cases} -1.8276 + 0.0178\,T - 1.5544 \times 10^{-5}\,T^2 + \\ + 4.5246 \times 10^{-9}\,T^3,\ T \in [125\text{K}\ 1273\text{K}] \\ 5.0 \times 10^{-6}/\text{K},\ T > 1273\text{K} \end{cases} \quad (16)$$

The temperature-dependent fiber/matrix interface debonded energy of $\gamma_d(T)$ and the matrix fracture energy of $\gamma_m(T)$ can be described using the following equations. [31]

$$\gamma_d(T) = \gamma_{do}\left[1 - \frac{\int_{T_o}^{T} C_P(T)\,dT}{\int_{T_o}^{T_m} C_P(T)\,dT}\right] \quad (17)$$

$$\gamma_m(T) = \gamma_{mo}\left[1 - \frac{\int_{T_o}^{T} C_P(T)\,dT}{\int_{T_o}^{T_m} C_P(T)\,dT}\right] \quad (18)$$

where T_o denotes the reference temperature; T_m denotes the fabricated temperature; γ_{do} and γ_{mo} denote the interface debonded energy and matrix fracture energy at the reference temperature of T_o; and $C_P(T)$ can be described using the following equation.

$$C_p(T) = 76.337 + 109.039 \times 10^{-3}\,T - 6.535 \times 10^{5}\,T^{-2} - 27.083 \times 10^{-6}\,T^2 \quad (19)$$

The effects of fiber volume fraction, interface shear stress, interface frictional coefficient, interface debonded energy and matrix fracture energy on the temperature-dependent proportional limit stress and interface debonded length are discussed.

Effect of fiber volume fraction on proportional limit stress and fiber/matrix interface debonding

The proportional limit stress (σ_{PLS}) and the fiber/matrix interface debonded length (l_d/r_f) versus the temperature curves for different fiber volume fraction (i.e., V_f = 30 % and 35 %) are shown in Figure 1.

When the fiber volume fraction is V_f = 30 %, the proportional limit stress increases from σ_{PLS} = 48 MPa at T = 973 K to σ_{PL} = 103 MPa at T = 1273 K; and the fiber/matrix interface debonded length increases from l_d/r_f = = 0.68 to l_d/r_f = 4.5.

When the fiber volume fraction is V_f = 35 %, the proportional limit stress increases from σ_{PLS} = 47 MPa at T = 973 K to σ_{PLS} = 113 MPa at T = 1273 K; and the fiber/matrix interface debonded length increases from l_d/r_f = = 0.08 to l_d/r_f = 3.9.

Effect of fiber/matrix interface shear stress on proportional limit stress and fiber/matrix interface debonding

The proportional limit stress (σ_{PLS}) and the fiber/matrix interface debonded length (l_d/r_f) versus the temperature curves for different fiber/matrix interface shear stress (i.e., τ_0 = 30 and 40 MPa) are shown in Figure 2.

When the fiber/matrix interface shear stress is τ_0 = = 30 MPa, the proportional limit stress increases from σ_{PLS} = 65 MPa at T = 973 K to σ_{PLS} = 115 MPa at T = = 1273 K; and the fiber/matrix interface debonded length increases from l_d/r_f = 1.4 to l_d/r_f = 4.2.

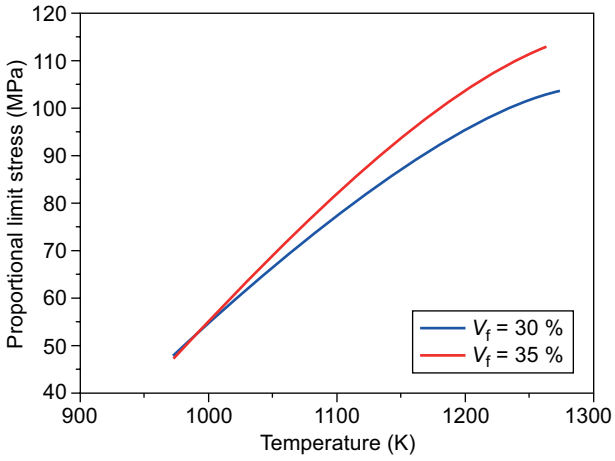

a)

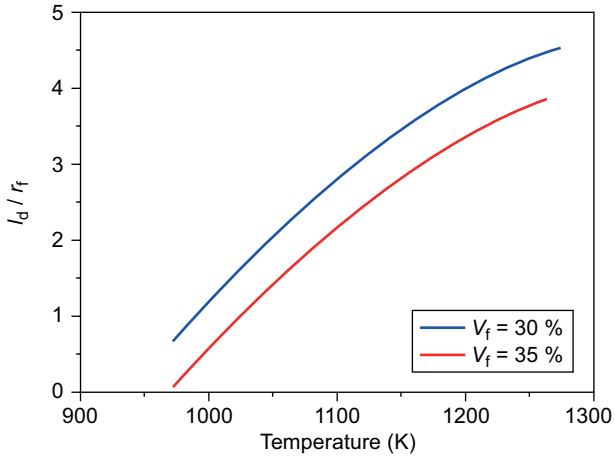

b)

Figure 1. The effect of fiber volume fraction (i.e., V_f = 30 % and 35 %) on: a) the proportional limit stress versus temperature curves; b) the interface debonding length (l_d/r_f) versus temperature curves of C/SiC composite.

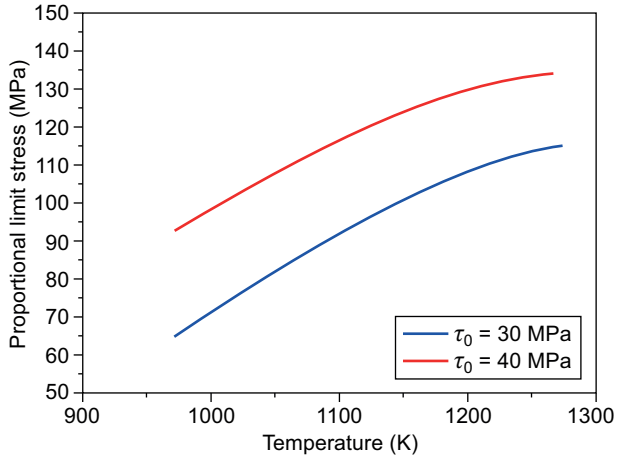

a)

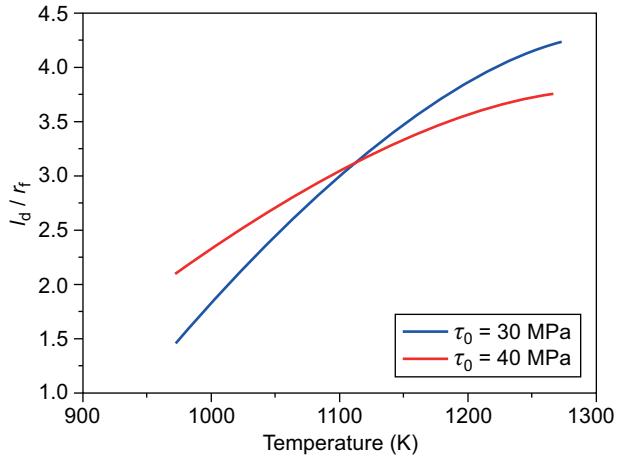

b)

Figure 2. The effect of fiber volume fraction (i.e., τ_0 = 30 and 40 MPa) on: a) the proportional limit stress versus temperature curves; b) the interface debonding length (l_d/r_f) versus temperature curves of C/SiC composite.

When the fiber/matrix interface shear stress is τ_0 = = 40 MPa, the proportional limit stress increases from σ_{PLS} = 93 MPa at T = 973 K to σ_{PLS} = 134 MPa at T = = 1273 K; and the fiber/matrix interface debonded length increases from l_d/r_f = 2.1 to l_d/r_f = 3.7.

Effect of fiber/matrix interface frictional coefficient on proportional limit stress and fiber/matrix interface debonding

The proportional limit stress (σ_{PLS}) and the fiber/matrix interface debonded length (l_d/r_f) versus the temperature curves for different interface frictional coefficient (i.e., μ = 0.03 and 0.05) are shown in Figure 3.

When the fiber/matrix interface frictional coefficient is μ = 0.03, the proportional limit stress increases from σ_{PLS} = 84 MPa at T = 973 K to σ_{PLS} = 131 MPa at T = 1273 K; and the fiber/matrix interface debonded length increases from l_d/r_f = 1.9 to l_d/r_f = 3.8.

When the fiber/matrix interface frictional coefficient is μ = 0.05, the proportional limit stress increases from σ_{PLS} = 65 MPa at T = 973 K to σ_{PLS} = 127 MPa at T = = 1273 K; and the interface debonded length increases from l_d/r_f = 1.5 to l_d/r_f = 3.9.

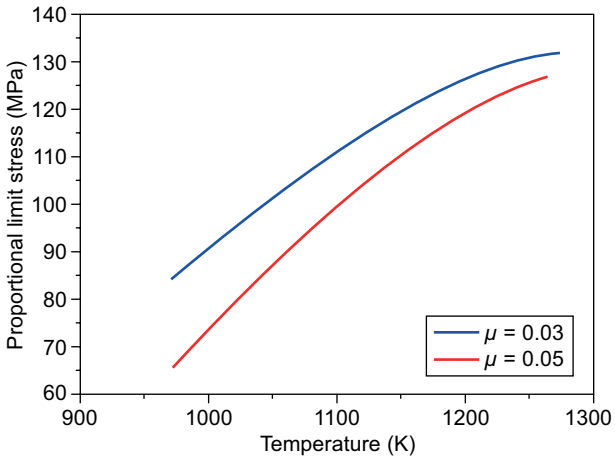

a)

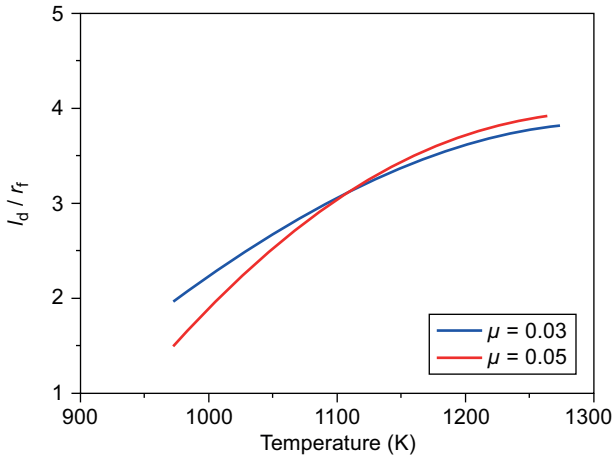

b)

Figure 3. The effect of interface frictional coefficient (i.e., μ = = 0.03 and 0.05) on: a) the proportional limit stress versus temperature curves; b) the interface debonding length (l_d/r_f) versus temperature curves of C/SiC composite.

Effect of fiber/matrix interface debonded energy on proportional limit stress and fiber/matrix interface debonding

The proportional limit stress (σ_{PLS}) and the fiber/matrix interface debonded length (l_d/r_f) versus the temperature curves for different fiber/matrix interface debonded energy (i.e., γ_d = 0.3 and 0.5 J·m^{-2}) are shown in Figure 4.

When the fiber/matrix interface debonded energy is γ_d = 0.3 J·m^{-2}, the proportional limit stress increases from σ_{PLS} = 102 MPa at T = 973 K to σ_{PLS} = 139 MPa at T = = 1273 K; and the fiber/matrix interface debonded length increases from l_d/r_f = 1.3 to l_d/r_f = 3.3.

When the fiber/matrix interface debonded energy is $\gamma_d = 0.5$ J·m^{-2}, the proportional limit stress increases from $\sigma_{PLS} = 110$ MPa at $T = 973$ K to $\sigma_{PLS} = 143$ MPa at $T = 1273$ K; and the fiber/matrix interface debonded length increases from $l_d/r_f = 0.9$ to $l_d/r_f = 3.0$.

When the matrix fracture energy is $\gamma_m = 30$ J·m^{-2}, the proportional limit stress increases from $\sigma_{PLS} = 79$ MPa at $T = 973$ K to $\sigma_{PLS} = 126$ MPa at $T = 1273$ K; and the fiber/matrix interface debonded length increases from $l_d/r_f = 2.2$ to $l_d/r_f = 4.7$.

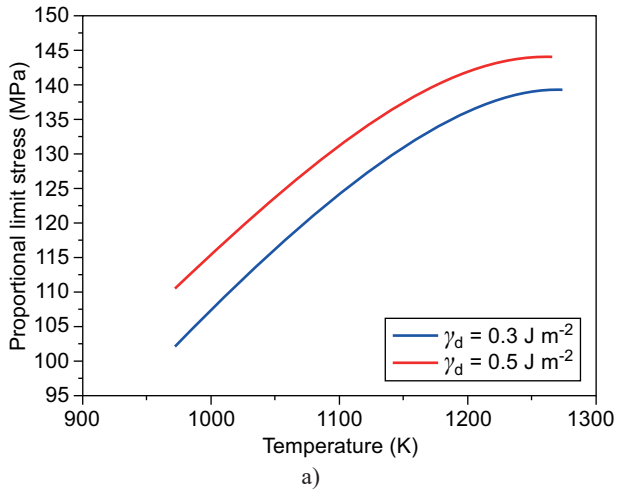

a)

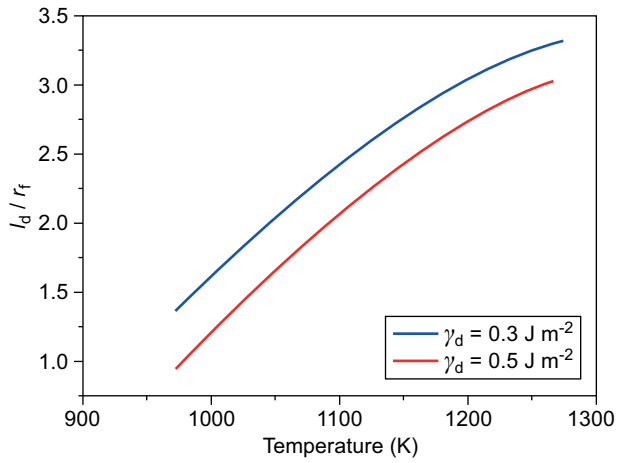

b)

Figure 4. The effect of interface debonded energy (i.e., $\gamma_d = 0.3$ and 0.5 J·m^{-2}) on: a) the proportional limit stress versus tem-perature curves; b) the interface debonding length (l_d/r_f) versus temperature curves of C/SiC composite.

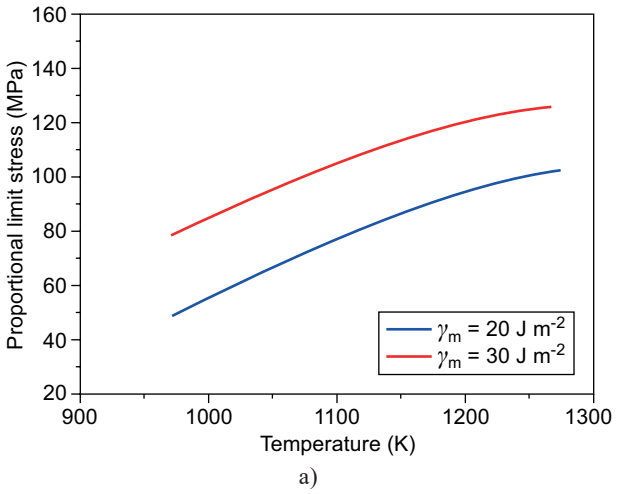

a)

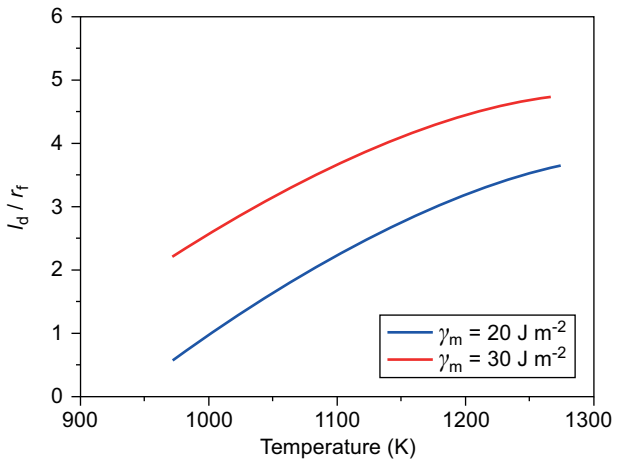

b)

Figure 5. The effect of interface debonded energy (i.e., $\gamma_m = 20$ and 30 J·m^{-2}) on: a) the proportional limit stress versus tem-perature curves; b) the interface debonding length (l_d/r_f) versus temperature curves of C/SiC composite.

Effect of matrix fracture energy on proportional limit stress and fiber/matrix interface debonding

The proportional limit stress (σ_{PLS}) and the fiber/matrix interface debonded length (l_d/r_f) versus the temperature curves for different matrix fracture energy (i.e., $\gamma_m = 20$ and 30 J·m^{-2}) are shown in Figure 5.

When the matrix fracture energy is $\gamma_m = 20$ J·m^{-2}, the proportional limit stress increases from $\sigma_{PLS} = 49$ MPa at $T = 973$ K to $\sigma_{PLS} = 102$ MPa at $T = 1273$ K; and the fiber/matrix interface debonded length increases from $l_d/r_f = 0.59$ to $l_d/r_f = 3.6$.

EXPERIMENTAL

Yang et al. [32] investigated the tensile behavior of 2D T300-C/SiC composite at elevated temperature. The C/SiC composite was fabricated using the chemical vapor infiltration (CVI) method with the pyrolytic carbon interphase of 1.5 ~ 2.0 μm. The fiber volume fraction is 40 %. The tensile tests were performed under the displacement control and the loading speed was 0.3 mm·min^{-1}. The tensile stress-strain curves of 2D C/SiC composite at elevated temperatures of $T = 973$ K and 1273 K are shown in Figure 6. The tensile

stress-strain response of 2D C/SiC composite exhibits obviously non-linearly. At an elevated temperature of T = 973 K, the composite proportional limit stress is about σ_{PLS} = 50 MPa, and the composite tensile strength is σ_{UTS} = 232 MPa with the failure strain of ε_f = 0.25 %; at elevated temperature of T = 1273 K, the composite proportional limit stress is about σ_{PLS} = 80 MPa, and the composite tensile strength is σ_{UTS} = 271 MPa with the failure strain of ε_f = 0.33 %. The experimental and theoretical predicted proportional limit stress and the fiber/matrix interface debonded length versus the temperature curves are shown in Figure 7. With increasing of the temperature, the proportional limit stress of 2D C/SiC composite increases from σ_{PLS} = 48 MPa at T = 973 K to σ_{PLS} = 82 MPa at T = 1273 K; and the fiber/matrix interface debonded length increases from l_d/r_f = 2.7 to l_d/r_f = 6.3.

CONCLUSIONS

In this paper, the temperature-dependent proportional limit stress of C/SiC composite has been investigated using the energy balance approach. The relationships between the proportional limit stress, fiber/matrix interface debonding and temperature have been established. The effects of fiber volume fraction, fiber/matrix interface shear stress, interface frictional coefficient, interface debonded energy and matrix fracture energy on the proportional limit stress and fiber/matrix interface debonding length versus temperature curves have been discussed. The experimental proportional limit stress and interface debonding length of 2D C/SiC composite at elevated temperatures of 973 K and 1273 K have been predicted.

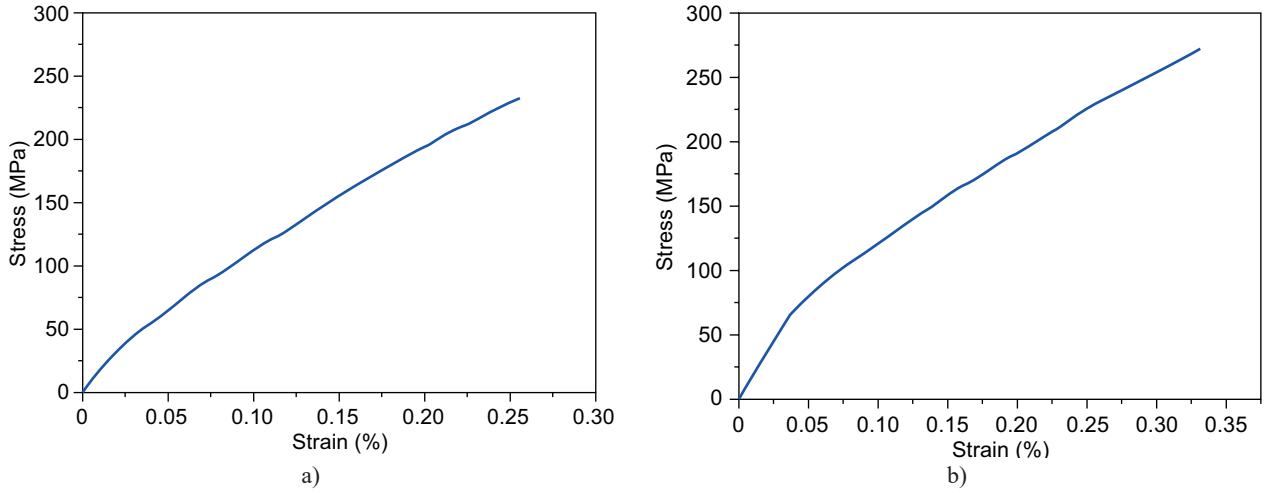

Figure 6. The tensile stress-strain curves of 2D C/SiC composite at: a) T = 973 K; and b) T = 1273 K.

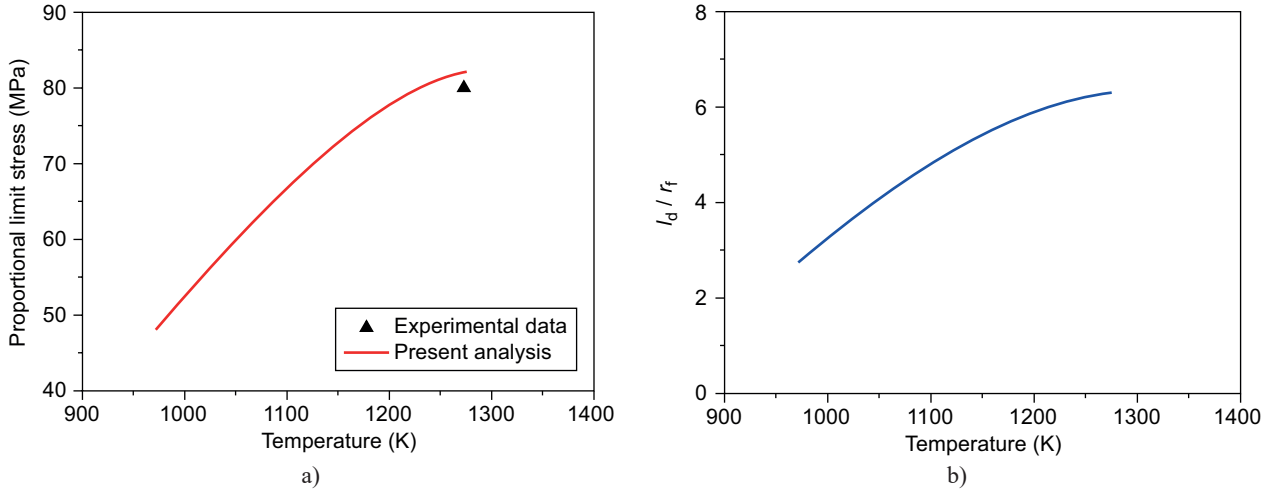

Figure 7. The experimental and theoretical proportional limit stress versus temperature curves (a); and the interface debonded length (l_d/r_f) versus temperature curves of 2D C/SiC composite (b).

- With increasing temperature, the proportional limit stress of C/SiC composite increases due to the increasing of the fiber/matrix interface shear stress and decreasing of thermal residual stress.
- With increasing fiber volume fraction, interface shear stress, interface debonded energy and matrix fracture energy, the temperature-dependent proportional limit stress of C/SiC composite increases.

Acknowledgements

The work reported here is supported by the Fundamental Research Funds for the Central Universities (Grant No. NS2019038).

REFERENCES

1. Christin F. (2002): Design, fabrication, and application of thermostructural composites (TSC) like C/C, C/SiC, and SiC/SiC composites. *Advanced Engineering Materials*, *4*(12), 903-912. Doi: 10.1002/adem.200290001
2. Naslain R. (2004): Design, preparation and properties of non-oxide CMCs for application in engines and nuclear reactors: an overview. *Composites Science and Technology*, *64*(2), 155-170. Doi: 10.1016/S0266-3538(03)00230-6
3. Schmidt S., Beyer S., Knabe H., Immich H., Meistring R., Gessler A. (2004): Advanced ceramic matrix composite materials for current and future propulsion technology applications. *Acta Astronautica*, *55*(3-9), 409-420. Doi: 10.1016/j.actaastro.2004.05.052
4. DiCarlo J. A., van Roode M. (2006): Ceramic composite development for gas turbine engine hot section components. in: *ASME Turbo Expo 2006: Power for Land, Sea, and Air*. American Society of Mechanical Engineers. pp. 221-231. Doi: 10.1115/GT2006-90151
5. Watanabe F., Nakamura T., Shinohara K. I. (2016). The application of ceramic matrix composite to low pressure turbine blade. In: *ASME Turbo Expo 2016: Turbomachinery Technical Conference and Exposition*. American Society of Mechanical Engineers. pp. V006T02A003-V006T02A003. Doi: 10.1115/GT2016-56614
6. Li L. (2015): Micromechanical Modeling for Tensile Behaviour of Carbon Fiber − Reinforced Ceramic − Matrix Composites. *Applied Composite Materials*, *22*(6), 773-790. Doi: 10.1007/s10443-014-9435-y
7. Li L. (2018): Modeling for monotonic and cyclic tensile stress-strain behavior of 2D and 2.5D woven C/SiC ceramic-matrix composites. *Mechanics of Composite Materials*, *54*(2), 165-178. Doi: 10.1007/s11029-018-9729-5
8. Li L. (2018). *Damage, Fracture and Fatigue in Ceramic-Matrix Composites*. Springer Nature Singapore Pte Ltd. Doi: 10.1007/978-981-13-1783-5
9. Jenkins M. G., Zawada L. P. (2001). Elastic Modulus and Proportional Limit Stress in Ceramic Matrix Composites: Comparison of Methods and Results. In: *25th Annual Conference on Composites, Advanced Ceramics, Materials, and Structures: A: Ceramic Engineering and Science Proceedings*. Hoboken, NJ, USA: John Wiley & Sons, Inc. pp. 502-511. Doi: 10.1002/9780470294680.ch58
10. Liu S., Zhang L., Yin X., Liu Y., Cheng L. (2014): Proportional limit stress and residual thermal stress of 3D SiC/SiC composite. *Journal of Materials Science & Technology*, *30*(10), 959-964. Doi: 10.1016/j.jmst.2014.08.004
11. Aveston J. (1971). The properties of fiber composites. In *Conf. Proc. National Physical Lab.* IPC Science and Technology Press. pp. 15-26.
12. Aveston J., Kelly A. (1973): Theory of multiple fracture of fibrous composites. *Journal of Materials Science*, *8*(3), 352-362. Doi: 10.1007/BF00550155
13. Budiansky B., Hutchinson J. W., Evans A. G. (1986): Matrix fracture in fiber-reinforced ceramics. *Journal of the Mechanics and Physics of Solids*, *34*(2), 167-189. Doi: 10.1016/0022-5096(86)90035-9
14. Kuo W. S., Chou T. W. (1995): Multiple Cracking of Unidirectional and Cross-PlyCeramic Matrix Composites. *Journal of the American Ceramic Society*, *78*(3), 745-755. Doi: 10.1111/j.1151-2916.1995.tb08242.x
15. Sutcu M., Hillig W. B. (1990): The effect of fiber-matrix debond energy on the matrix cracking strength and the debond shear strength. *Acta Metallurgica et Materialia*, *38*(12), 2653-2662. Doi: 10.1016/0956-7151(90)90278-O
16. Chiang Y. C. (2001): On fiber debonding and matrix cracking in fiber-reinforced ceramics. *Composites Science and Technology*, *61*(12), 1743-1756. Doi: 10.1016/S0266-3538(01)00078-1
17. Li L. (2017):Synergistic effects of fiber debonding and fracture on matrix cracking in fiber-reinforced ceramic-matrix composites. *Materials Science and Engineering: A*, *682*, 482-490. Doi: 10.1016/j.msea.2016.11.077
18. Marshall D. B., Cox B. N., Evans A. G. (1985): The mechanics of matrix cracking in brittle-matrix fiber composites. *Acta metallurgica*, *33*(11), 2013-2021. Doi: 10.1016/0001-6160(85)90124-5
19. Marshall D. B., Cox B. N. (1987): Tensile fracture of brittle matrix composites: influence of fiber strength. *Acta metallurgica*, *35*(11), 2607-2619. Doi: 10.1016/0001-6160(87)90260-4
20. McCartney L. N. (1987): Mechanics of matrix cracking in brittle-matrix fibre-reinforced composites. *Proceedings of the Royal Society of London. A. Mathematical and Physical Sciences*, *409*(1837), 329-350. Doi: 10.1098/rspa.1987.0019
21. Chiang Y. C., Wang A. S. D., Chou T. W. (1993): On matrix cracking in fiber reinforced ceramics. *Journal of the Mechanics and Physics of Solids*, *41*(7), 1137-1154. Doi: 10.1016/0022-5096(93)90087-V
22. Danchaivijit S., Shetty D. K. (1993): Matrix Cracking in Ceramic-Matrix Composites. *Journal of the American Ceramic Society*, *76*(10), 2497-2504. Doi: 10.1111/j.1151-2916.1993.tb03972.x
23. Thouless M. D., Evans, A. G. (1988): Effects of pull-out on the mechanical properties of ceramic-matrix composites. *Acta Metallurgica*, *36*(3), 517-522. Doi: 10.1016/0001-6160(88)90083-1
24. Kim R. Y., Pagano N. J. (1991): Crack Initiation in Unidirectional Brittle-Matrix Composites. *Journal of the American Ceramic Society*, *74*(5), 1082-1090. Doi: 10.1111/j.1151-2916.1991.tb04346.x
25. Dutton R. E., Pagano N. J., Kim R. Y., Parthasarathy T. A. (2000): Modeling the Ultimate Tensile Strength of Unidirectional Glass-Matrix Composites. *Journal of the American Ceramic Society*, *83*(1), 166-174. Doi: 10.1111/j.1151-2916.2000.tb01166.x

26. Barsoum M. W., Kangutkar P., Wang A. S. D. (1992): Matrix crack initiation in ceramic matrix composites Part I: Experiments and test results. *Composites Science and Technology*, *44*(3), 257-269. Doi: 10.1016/0266-3538(92)90016-V
27. Reynaud P., Rouby D., Fantozzi G. (1994): Effects of interfacial evolutions on the mechanical behavior of ceramic matrix composites during cyclic fatigue. *Scripta Metallurgica et Materialia;(United States)*, *31*(8). Doi: 10.1016/0956-716X(94)90527-4
28. Sauder C., Lamon J., Pailler R. (2004): The tensile behavior of carbon fibers at high temperatures up to 2400 C. *Carbon*, *42*(4), 715-725. Doi: 10.1016/j.carbon.2003.11.020
29. Snead L. L., Nozawa T., Katoh Y., Byun T. S., Kondo S., Petti D. A. (2007): Handbook of SiC properties for fuel performance modeling. *Journal of Nuclear Materials*, *371*(1-3), 329-377. Doi: 10.1016/j.jnucmat.2007.05.016
30. Pradere C., Sauder C. (2008): Transverse and longitudinal coefficient of thermal expansion of carbon fibers at high temperatures (300–2500 K). *Carbon*, *46*(14), 1874-1884. Doi: 10.1016/j.carbon.2008.07.035
31. Wang R., Li W., Li D., Fang D. (2015): A new temperature dependent fracture strength model for the ZrB_2–SiC composites. *Journal of the European Ceramic Society*, *35*(10), 2957-2962. Doi: 10.1016/j.jeurceramsoc.2015.03.025
32. Yang C. P., Zhang L., Wang B., Huang T., Jiao G. Q. (2017): Tensile behavior of 2D-C/SiC composites at elevated temperatures: Experiment and modeling. *Journal of the European Ceramic Society*, *37*(4), 1281-1290. Doi: 10.1016/j.jeurceramsoc.2016.11.011